Accepted Manuscript

Antiproliferative and apoptotic activities of sequence-specific histone acetyltransferase inhibitors

Zutao Yu, Junichi Taniguchi, Yulei Wei, Ganesh N. Pandian, Kaori Hashiya, Toshikazu Bando, Hiroshi Sugiyama

PII: S0223-5234(17)30483-X

DOI: 10.1016/j.ejmech.2017.06.037

Reference: EJMECH 9532

To appear in: *European Journal of Medicinal Chemistry*

Received Date: 29 March 2017

Revised Date: 30 May 2017

Accepted Date: 22 June 2017

Please cite this article as: Z. Yu, J. Taniguchi, Y. Wei, G.N. Pandian, K. Hashiya, T. Bando, H. Sugiyama, Antiproliferative and apoptotic activities of sequence-specific histone acetyltransferase inhibitors, *European Journal of Medicinal Chemistry* (2017), doi: 10.1016/j.ejmech.2017.06.037.

Antiproliferative and Apoptotic Activities of Sequence-Specific Histone Acetyltransferase Inhibitors

Zutao Yu[a], Junichi Taniguchi[a], Yulei Wei[a], Ganesh N. Pandian[b], Kaori Hashiya[a], Toshikazu Bando[a*], Hiroshi Sugiyama[a,b*]

[a]*Department of Chemistry, Graduate School of Science, Kyoto University Kitashirakawa-Oiwakecho, Sakyo-ku, Kyoto 606-8502 (Japan)*

[b]*Institute for Integrated Cell-Material Sciences (WPI-iCeMS), Kyoto University Yoshida-Ushinomiyacho, Sakyo-ku, Kyoto 606-8501 (Japan).*

ABSTRACT

In parallel to monomeric epigenetic regulators, sequence-specific epigenetic regulators represent versatile synthetic dual-target ligands that achieve regulatory control over multi-gene networks. Development of DNA-binding domain (DBD)-HDAC inhibitors and DBD-HAT activators, which result in increased histone acetylation, has become one promising research field. However, there is no report regarding the gene regulatory pattern by sequence-specific epigenetic repressor. We report here for the first time, the synthesis of DBD-HAT inhibitors and demonstrate that these conjugates could retain their dual-target activity using predicted working model of thermal stability assay and *in vitro* HAT activity assay. Evaluation of antiproliferative activity in cancer cells showed that **2** (with a medium linker length of 13-atom) exhibited the highest antiproliferative activity in p53 wild-type cancer cell lines (IC_{50} of 1.8-2.6 μM in A549 and MV4-11 cells) and not in p53 mutant cancer cell lines. A mechanistic investigation using microarray analysis and an apoptotic assay showed that the antiproliferative effect of **2** occurred *via* the up-regulation of p53 target genes, and the subsequent initiation of p53-dependent apoptosis. Our research on sequence-specific dual-target epigenetic repressor offers us an alternative way to modulate HAT-governed therapeutically important genes and contributes to offer a fresh insight into antitumor therapeutics.

***Keywords*:**

Epigenetics; Sequence specificity; Polyamide; HAT inhibitor; Antiproliferation; Apoptosis

***Abbreviations*:** HAT, histone acetyltransferase; DBD, DNA-binding domain; HDAC, histone deacetylase; PIP, pyrrole-imidazole polyamides; DMSO, dried dimethylsulfoxide; IPA, ingenuity pathway analysis; GSEA, gene set enrichment analysis; KEGG, Kyoto encyclopedia of genes and genomes; ESI-TOF MS, electrospray ionization time-of-flight mass spectrometry, DMF, dimethylformamide; HPLC, high performance liquid chromatography; FBS, fetal bovine serum;

***Corresponding author.** Department of Chemistry, Graduate School of Science, Kyoto University Kitashirakawa-Oiwakecho, Sakyo-ku, Kyoto 606-8502 (Japan)

***E-mail addresses*:** bando@kuchem.kyoto-u.ac.jp (T. Bando), hs@kuchem.kyoto-u.ac.jp (H. Sugiyama).

1. Introduction

Among epigenetic families, histone acetylation has been identified as a key histone marker that switches on gene expression, ant its dysregulation are associated with substantial diseases [1]. Several epigenetic agents, such as histone deacetylase (HDAC) inhibitors (SAHA and TSA), histone acetyltransferase (HAT) activators (CTB and CTPB), and HAT inhibitors (C646 and anacardic acid), have been approved or are in preclinical development as they showed promising therapeutic efficacy [2-5]. Along with the extensively studied monomeric epigenetic regulators, sequence-specific epigenetic activators have recently gained prominence as an emerging class of versatile synthetic dual-target ligands capable of having regulatory control over multi-gene networks (**Figure 1**) [6, 7].

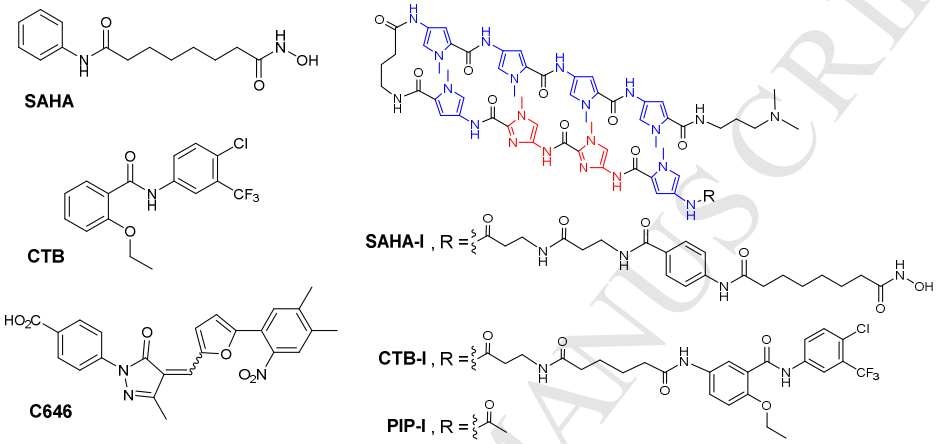

Figure 1. Chemical structures of the HDAC inhibitors SAHA and **SAHA-I**, HAT activators CTB and **CTB-I**, and HAT inhibitor C646.

Our lab has focused on sequence-specific epigenetic activators that involve conjugation of epigenetic modulators with DNA-binding domains (DBDs), i.e., pyrrole-imidazole polyamides (PIPs) [8]. PIPs are programmable DNA minor groove binders with the ability to recognize and bind specific DNA sequences strongly (with the Py/Py pair recognizing A/T or T/A, Py/Im recognizing C/G, and Im/Py recognizing G/C**)** [9]. By incorporating a variable 8-ring PIP moiety, compound library of both HDAC inhibitor conjugates (SAHA-PIP) [10], we showed gene-specific histone acetylation and downstream gene activation in living cells. Promisingly, after conjugation with SAHA, the **PIP-I** sequence **(**DNA-binding sequence, 5′–WWCCWW–3′, W = A/T**)** exhibited the highest potential to upregulate *SOX2*, *OCT4* and *NANOG*, which are responsible for iPS cell formation and maintenance (**Figure 1**) [11]. More interestingly, when SAHA was replaced with CTB, **CTB-I** showed a gene activation pattern that was similar to that of **SAHA-I**, although it targeted a different epigenetic regulator [12].

In contrast with sequence-specific epigenetic activators, such as SAHA-PIP and CTB-PIP which functionally resulted in gene activation, no sequence-specific epigenetic repressor has been reported. In this work, we constructed dual-function and sequence-specific HAT inhibitor *via* C646 conjugation with **PIP-I,** for the development of novel cancer therapies [5]. Through independent lines of evidence, we characterize the activity mode of sequence-specific HAT inhibitor conjugates and demonstrate the anti-proliferative activities in cancer cell lines including A549 and MV4-11 cells. Microarray analysis and an apoptotic assay revealed the initiation of apoptosis caused by the upregulation of p53 target genes as the mechanism behind the antiproliferative effect of in cancer

cells. Because HAT enzymes are known to regulate the genes associated with tumorigenesis, our study suggests the novel chemical approach to modulate the gene-regulatory pathway in a sequence-specific manner.

2. Results and discussion

2.1 Design and synthesis

C646, which was reported by Philip A. Cole through silica screening, is the most potent HAT inhibitor available currently. C646 inhibits p300 with a K_i value of 400 nM *in vitro* and significantly downregulates histone acetylation in human lung cancer cells and melanoma cells [5]. C646 contains a carboxyl group, and its amide analogs or propargylamine conjugates exhibit the same level of HAT inhibitory activity, which implies that PIP conjugation at the carboxyl site is a good choice, while maintaining HAT inhibitory activity [13].

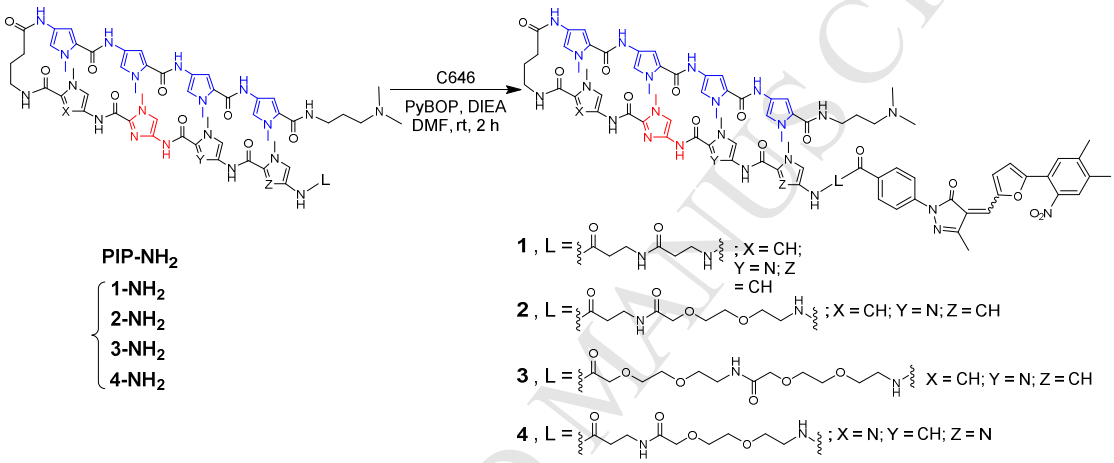

Scheme 1. Structural design of PIP conjugates of the HAT inhibitor C646 (C646-PIP).

Inspired by the 8-ring **PIP-I**, we performed **PIP-I** conjugation with the HAT inhibitor C646 (**C646-I**) [12]. The linker region between the functional group and PIP might affect its binding affinity and functional effect. Our group reported six kinds of linkers of SAHA-PIP, and revealed that a linker length of 12-atom yielded maximum expression of *OCT3/4* [14]. In this work, after taking linker length and chain flexibility into consideration, we designed **C646-I** conjugates with three types of linkers, i.e., a shorter linker (8-atom, **1**), a moderate linker (13-atom, **2**), and a longer linker (18-atom, **3**) (**Scheme 1**). Concomitantly, an alternative PIP sequence ligated with C646 (**4**) was also designed, to investigate the PIP sequence/activity relationship.

C646-PIP synthesis started from pyrrole-oxime resin [15]. Using an 11-step Fmoc-protected solid-phase synthesis, four PIPs were synthesized and cleaved by *N*,*N*-dimethylamine. After purification using a reverse-phase flash column, our target compounds were synthesized by combining the terminal amino group of the PIP chain with commercially available C646, which contains a carboxyl group, with the help of the coupling agent PyBOP (Supplementary Data **S2**). These conjugates were then purified in high yield.

2.2 Determination of the DNA-binding affinity

A predictive working system in molecular level to evaluate dual-target conjugates would accelerate the research progress and obviate unintended bioactivity in the early research phase.

Since C646-PIP conjugates contain DNA binding moiety and HAT inhibitor, we presume that thermal stability assay and HAT activity assay might be suitable for preliminary evaluation. We first performed T_m assay to test thermal stabilization of dual-function conjugates-DNA complexes [16].

Table 1. Results of thermal stability assay

Conjugates	Match sequence ODN1: 5'-ACTTATTCCATATAGA-3' ODN2: 3'-TGAATAAGGTATATCT-5' T_m = 32.5 ℃ (± 0.1)			Mismatch sequence ODN3: 5'-ACTTATCCACTATAGA-3' ODN4: 3'-TGAATAGGTGATATCT-5' T_m = 34.3 ℃ (± 0.1)		
	T_m/℃	ΔT_m/℃[a]	$\Delta\Delta T_m$/℃	T_m/℃	ΔT_m/℃	$\Delta\Delta T_m$/℃[b]
1	49.4 (± 0.1)	16.9	—	45.3 (± 0.1)	11.0	5.9
2	50.6 (± 0.1)	18.1	—	45.8 (± 0.1)	11.5	6.6
3	50.9 (± 0.1)	18.4	—	46.5 (± 0.1)	12.2	6.2
4	46.1 (± 0.1)	13.6	—	55.2 (± 0.1)	20.9	-7.3

[a] $\Delta T_m = \Delta T_m$(dsDNA + PIP) - ΔT_m(dsDNA); [b] $\Delta\Delta T_m = \Delta T_m$(match) - ΔT_m(mismatch)

As shown in **Table 1**, conjugates **1-3** stabilized match ODN1/2 with ΔT_m of 16.9, 18.1, and 18.4 ℃ respectively. Upon the incubation with mismatch ODN3/4, conjugates **1-3** showed a far weaker binding affinity (ΔT_m of 11.0-12.2 ℃), which demonstrated that conjugates **1-3** could discriminate between match and mismatch sequence with binding sequence specificity ($\Delta\Delta T_m$) ranged from 5.9- 6.6 ℃. Regarding conjugate **4**, it also showed notable binding affinity to its match ODN3/4 with ΔT_m of 20.9 ℃and sequence specificity of ΔT_m of 7.3 ℃. These results confirmed that upon the conjugation with C646, PIP retained its high binding affinity and sequence specificity to targeted DNA sequences.

2.3 In vitro HAT activity assay

After conjugation with PIP, functional moieties, such as SAHA, CTB, and alkylating agents, still harbored their functional activity toward the primary targets (HDAC inhibition, HAT activation and DNA alkylation), with only a slight loss of activity [17]. Therefore, it is mandatory that the conjugation of **PIP-I** with C646 does not diminish the histone acetylation inhibitory activity. We then evaluated the HAT activity of all synthesized C646-PIP conjugates using a commercially available HAT activity kit. We used p300 as the HAT enzyme, as C646 showed high selectivity to p300 compared with a panel of similar functional enzymes, such as PCAF, GCN5, AANAT, Sas, Moz, and Rtt109 [5]. The HAT inhibitory activity was assessed using fluorescence absorption on a microreader using the H3 peptide and Ac-CoA as substrates. Besides, we also designed and evaluated anacardic acid, a widely used HAT inhibitor, and its conjugates with PIP in a predictive working system [18]. However, after PIP conjugation, they did not show any HAT inhibitory activity (Supplementary **S3** and **S4**). The conjugation of PIP blocked the binding of anacardic acid to the active pocket of p300, which might be responsible for the undesired outcome.

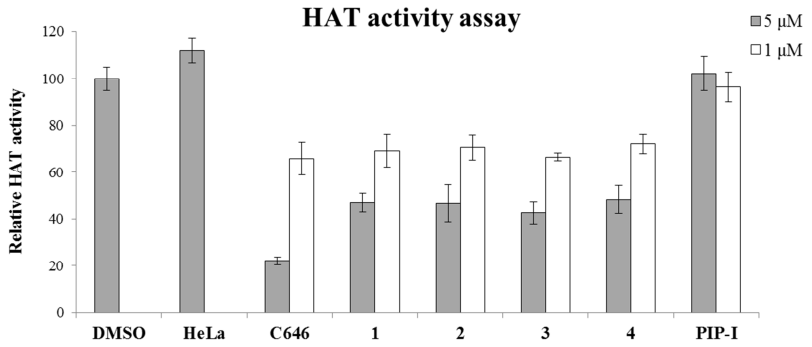

Figure 2. HAT inhibitory activity assay. The enzymatic activity of HAT was tested in the presence of C646, **1**, **2**, **3**, **4,** and **PIP-I**. Each effector was individually administered at two concentrations (1 and 5 μM) to the p300 enzyme using a HeLa cell nuclear extract as a positive control and the 0.5% DMSO group as a control group. $P<0.05$.

Our results showed an IC_{50} of 2.4 μM for C646, which is comparable with that reported previously [19]. As expected, the **PIP-I** sequence without C646 did not possess HAT inhibitory activity. Concomitantly, all C646-PIP derivatives, regardless of linker region and PIP sequence, maintained HAT inhibitory activity, with IC_{50} values around 3.9–4.2 μM. These data verify that C646-PIP preserved p300 inhibitory activity and the changes in PIP sequence had no obvious deleterious effects on IC_{50}. In addition, the inhibitory activity of C646-PIP was slightly decreased compared with the C646 monomer, which might be attributed to the constraints exhibited by PIP moiety over C646 binding to HAT.

2.4 Antiproliferative activity assay

Previously, antiproliferative activity of HAT inhibitors was shown in cancer cell lines [3, 20]. After a 10-day treatment, C646 exhibited an IC_{50} of 10.0, 6.0, and 6.3 μM in A549, H157, and H460 cells, respectively, as assessed by a clonogenic survival assay based on a published article [21]. Under ionizing radiation therapy, C646 radiosensitized lung cancer cells by enhancing the mitotic catastrophe. However, only a limited dose ratio enhancement of 1.2–1.4 fold was observed in this study to suggest the need to incorporate an alternative molecular design.

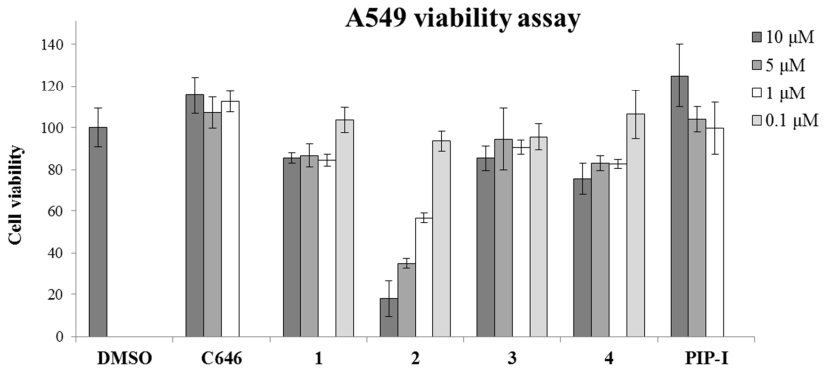

Figure 3. Cell viability assay in the A549 cell line using the WST-8 method. A549 cells were grown in 10% FBS/DMEM medium for 24 h. Subsequently, the medium was replenished with varying concentrations of C646-PIP conjugates (0.1, 1, 5, and 10 μM) for 96 h. The cell viability of A549 cells was measured using the WST-8 method. Each bar represents the mean ± SD from three wells. $P<0.05$.

Here, we studied the antiproliferative activity of C646-PIP using a cell viability assay in A549 cells [22]. In consistent with our notion, A549 cell viability was not affected by **PIP-I** and C646, even at the concentration of 10 μM, after 96 h of treatment (**Figure 3**). Treatment with C646-PIP conjugates led to cell inhibition, but the extent of activity varied considerably among conjugates with different linker lengths and PIP sequences.

Regarding the shared **PIP-I** sequence, **2** (moderate linker with a 13-atom distance) exhibited the highest antiproliferative activity, with an IC_{50} of 1.8 μM, in a dose-dependent manner. This implies that the length of the linker plays a pivotal role regarding its cellular effect, which was different from the simplified HAT inhibitory activity *in vitro*. If the linker length was too short (**1**), C646 may not be sufficiently free to bind to the active pocket of p300 while PIP bound to DNA. In contrast, a linker that was too long (**3**) may push C646 out of the localized region of PIP binding thereby hampering the sequence-specificity. **2** and **4** had the same linker length (13-atom distance), but different PIP sequences. However, **4** showed only a slight antiproliferative activity in A549 cells to imply that the **PIP-I** sequence is necessary for antiproliferative activity.

2.5 Microarray analysis

Microarray analysis has been used widely to identify underlying regulatory gene patterns [23]. In this work, whole-genome transcriptional profiling of the A549 cell line was performed using microarray analysis, according to the manufacturer's protocol [24]. **2** (2 μM) and **4** (2 μM) were added respectively, for 48 h. **4** did not exhibit a specific gene regulatory pattern, which was consistent with its low antiproliferative activity. After treatment with **2**, among the more than 50,000 transcripts identified, 310 target genes showed 1.5-fold changes in expression levels (P<0.05), with upregulation observed for 170 transcripts and downregulation detected for 140 transcripts. Genes detail information of microarray data up- and downregulated by treatment with **2** with levels >1.8-fold and <–1.8-fold changes (p<0.05) by Affymetrix gene expression console software (**Table 2)**.

Table 2. Genes detail information of microarray data up- and downregulated by treatment with **2**. Genes with >1.8-fold and <–1.8-fold changes (P<0.05). Uncharacterized transcripts were excluded from this table. Gene symbols in red color and green color are upregulated and downregulated p53 downstream targets, respectively.

Gene Symbol	Fold Change	Gene Symbol	Fold Change
SPATA18	2.98	*TP53INP1*	1.85
EDA2R	2.53	*CD70*	1.83
ABCA12	2.42	*FAS*	1.83
BTG2	2.35	*GDF15*	1.81
MIR3189	2.32	*GAS6-AS1*	1.81
CDKN1A	2.28	*ANKRD1*	1.81
SULF2	2.13	*DDB2*	1.80
WDR63	2.03	*NEFL*	1.80
FDXR	2.00	*SNORA9*	-1.81
MDM2	1.97	*ALDH1L2*	-1.86
UIMC1	1.94	*CARS*	-1.90
MIR4713	1.94	*ASNS*	-2.01
SESN1	1.91	*TAS2R30*	-2.01
SCARNA7	1.89	*STC2*	-2.34
MIR3685	1.89	*ULBP1*	-2.34
CYFIP2	1.88	*GUSBP3*	-2.63
POLH	1.88	*CHAC1*	-3.64

We performed an Ingenuity Pathway Analysis (IPA) of the differentially expressed genes, to gain a more precise global understanding of the underlying biological processes (**Figure 4a**) [25].

Interestingly, while **4** did not show potent and specific gene pattern regulations, treatment with **2** led to a strong enrichment of p53 target genes, such as *SPATA18* (2.98 fold), *BTG2* (2.35 fold), *FDXR* (2.00 fold), and *MDM2* (1.97 fold), among the top regulated transcripts. We then performed a Gene Set Enrichment Analysis (GSEA) of the significantly differentially regulated genes using the published gene expression profiles of p53 targets with gene sets of the Kyoto Encyclopedia of Genes and Genomes (KEGG) (Supplementary Data **S5**) [26]. Consistent with the IPA analysis, GSEA demonstrated that the p53 signaling pathway was predominantly enriched among all 185 gene sets identified, with an enrichment score of 0.67 and a *P* value <0.001(**Figure 4b**).

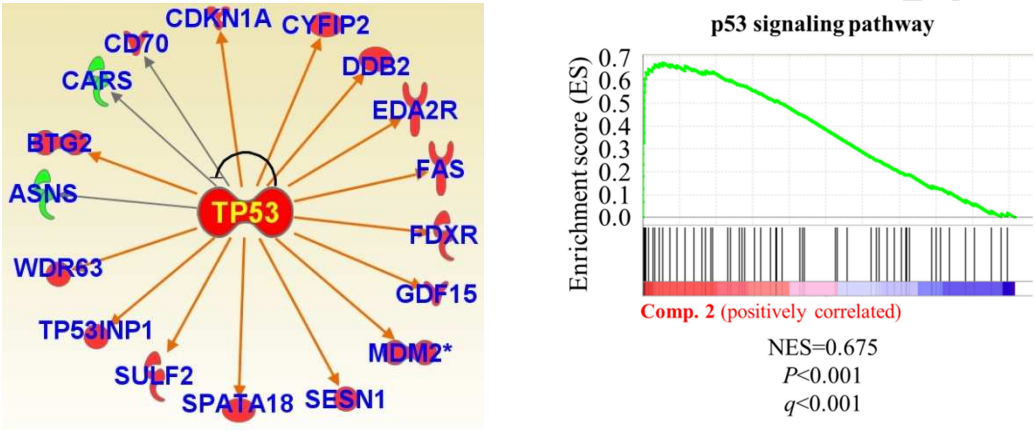

Figure 4. a) Significantly enriched target genes annotation in p53 by IPA. Targeting genes depicting the effect of **2** (compared with DMSO) the expression pattern of p53 pathway target genes in the technical duplicates of whole transcriptome analysis ($P<0.05$) regulated at least 1.8-fold. **b)** A Gene Set Enrichment Analysis (GSEA) was performed to assess whether genes that were differentially repressed by **2** were significantly associated with p53 direct effectors expression profiles of KEGG gene sets and gene symbols (GSEA database c2.cp.kegg.v5.2.symbols.gmt). The enrichment score clearly showed that the genes at the top of the ranked list were overrepresented in the reference gene set. $P<0.001$ and $q<0.001$.

A549 cells contain wild-type p53. Previous reports demonstrated that wild-type p53 plays a significant role in tumor inhibition. Stabilizing p53 and selectively activating p53 targets in p53 wild-type cells resulted in a pronounced antiproliferative effect by inducing cell-cycle arrest and apoptosis [27]. **SAHA-I** and **CTB-I** activated *SOX2*, *OCT4*, and *NANOG* in somatic human cells, while showing no antiproliferative activity, and treatment with **2** showed slight decreases of pluripotent genes after detail inspection of microarray data. Previous report demonstrated that downregulation of p53 pathway is required for efficient iPS cell reprogramming and maintenance [28]. Our data suggest that the inhibition of pluripotent genes might result in p53 pathway activation based on the microarray data. Furthermore, **2** showed weak antiproliferative activity in p53-mutant SW620 cells. Therefore, these results combined with the cell viability assay and microarray experiment discussed above led us to conclude that the antiproliferative activity caused by **2** in A549 cells was mainly attributable to the activation of p53 targeting genes.

2.6 Apoptotic assay

Among the many roles of tumor suppressor p53, the role of p53-dependent apoptosis in pathological conditions was identified and well-documented, especially in cancer [27]. The

microarray results led us to presume that p53-denpendent apoptosis might be the antiproliferative mechanism underlying the effects observed for **2**.

To confirm this hypothesis, cellular apoptosis was investigated via Annexin V-FITC assay, together with living cells and dead cells [29]. A549 cells were treated with **2** and **4** for 48 h. Subsequently, apoptotic, necrotic, and healthy cells were stained with three different fluorophores (Annexin V-FITC, ethidium homodimer III, and Hoechst 33342) (**Figure 5**).

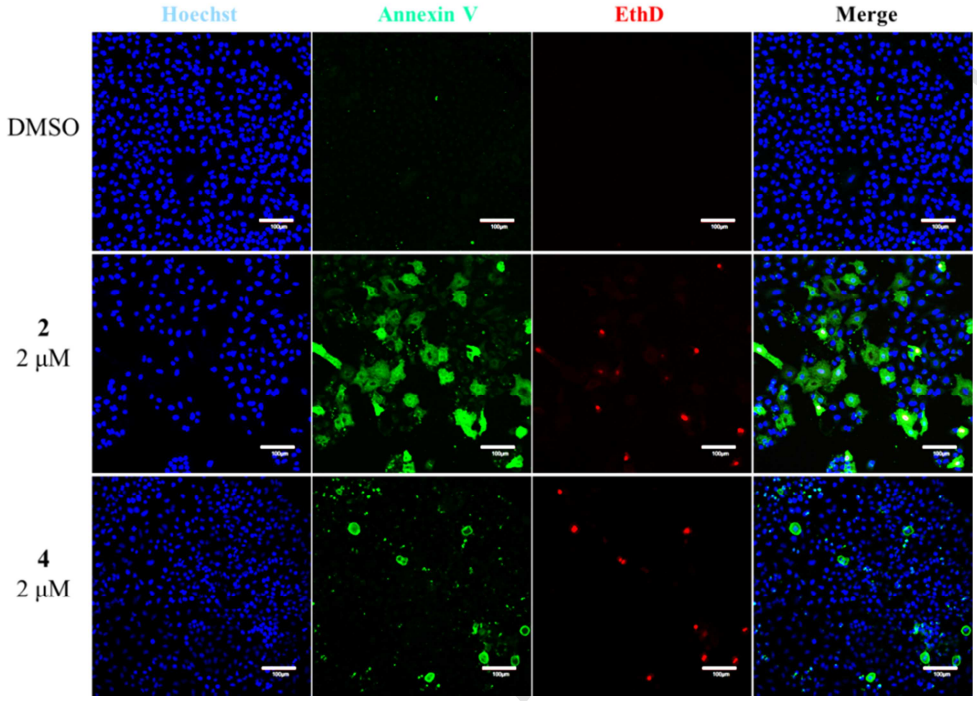

Figure 5. Effect of **2** and **4** on cellular apoptosis and necrotic activity. Representative images of apoptosis detection using fluorescence imaging. A549 cells were treated with DMSO, **2**, and **4** at 2 μM for 48 s. A confocal image showed Hoechst 33342 staining, Annexin V-FITC staining, ethidium homodimer III staining, and an overlay of the images. (Scale bars represent 100 μm).

In accordance with the IC_{50} of **2,** 2 μM **2** and **4** were applied to observe the process of cell death. In the control experiment (0.1% DMSO), apoptotic/dead cells were difficult to detect. Conversely, cultures treated with **2** showed more abundant apoptotic cells and an obvious subset of dead cells, which was consistent with the results of the cell viability assay described above. For **4**, most of the cells were in a healthy condition, and only a few necrotic cells and apoptotic cells were detected. As wild-type p53 plays a major role in A549 cell apoptosis, it is reasonable to assume that **2** activated p53 downstream targets and induced cell apoptosis, leading to programmed cell death.

To validate the role of p53 in antiproliferative and apoptotic activities of **2**, we further tested **2** in wild-type p53 cell line (MV4-11 cells) and mutant p53 cell lines (SW620 and MDA-MB-231 cells) for 96 h (Supplementary Data **S6**). Consistent with antiproliferative activity in A549 cells, **2** showed IC_{50} of 2.6 μM in MV4-11 cells. On the other hand, results showed that **2** had weak inhibitory activity in mutant p53 cell lines SW620 cells (78.4% cell viability) and MDA-MB-231 cells (69.3% cell viability) at the concentration of 10 μM. Above all, the antiproliferative and apoptotic activity of **2** might mainly mediated by wild-type p53 rather than mutant-p53.

3. Conclusions

In addition to DNA mutation, heritable phenotypes, such as the inactivation of tumor suppressor genes, can also be acquired by epigenetic modifications, including DNA methylation and histone modifications [30]. Inactivation of tumor suppressors and their downstream pathways, such as the p53 pathway, or activation of proto-oncogenes and their correspondent pathways, such as the RAS pathway, have been extensively studied to play a pivotal role in tumor initiation and development. In particular, wild-type p53 is popularly known as the guardian of the genome owing to its significant role in tumor inhibition. Stabilizing p53 and selectively activating the p53 pathway in p53 wild-type cells resulted in a pronounced antiproliferative effects *via* the induction of cell-cycle arrest and apoptosis [31]. In contrast, mutations in the p53 tumor suppressor gene are associated clinically with cancer stem cell progression and metastasis [32, 33].

In this study, we report for the first time about the synthesis and characterization of a new type of dual-functional conjugates comprised of a selective DNA-recognizing small molecule and a synthetic inhibitor of HAT activity. Our predicted working model about dual functionality, i.e., sequence-specific DNA binding and HAT inhibitory activity got substantiated using thermal stability assay and HAT activity assay, respectively. To evaluate the bioactivity of our dual-functional conjugates, we investigated the antiproliferative activities in p53 wild-type cell lines (A549 and MV4-11 cells) and p53 mutant cell lines (SW620 and MDA-MB-231 cells). Among C646-PIP derivatives synthesized, **2** (with a medium linker length of 13-atom) showed potent antiproliferative activity with an IC_{50} of 1.8-2.6 μM in A549 and MV4-11 cells. Additionally, the data acquired from microarray analysis and apoptosis assay, we demonstrated that the antiproliferative mechanism of **2** occurred *via* the activation of p53 target genes, which in turn triggered subsequent p53-dependent apoptosis. Potent antiproliferative activities and multi-gene network regulation observed in this research on sequence-specific dual-target epigenetic repressor offer us an alternative way to study and develop novel antitumor therapeutics.

4. Experimental section

4.1 General methods

Reagents and solvents were purchased from standard suppliers and used without further purification. HAT inhibitor C646 was purchased from Sigma-Aldrich (SML0002-25 mg). HPLC analysis were performed with a JASCO PU-2080 plus HPLC pump, a JASCO 807-IT HPLC UV/Vis detector, and a Chemcobond 5-ODS-H reversed-phase column (4.6×150 mm) in 0.1 % TFA in water using acetonitrile as the eluent at a flow rate of 1.0 mL min^{-1} under detection at 254 nm. Electrospray ionization Time-of-flight mass spectrometry (ESI-TOF MS) was performed on a Bio-TOF II (Bruker Daltonics) mass spectrometer by using positive ionization mode. Machine-assisted PIP syntheses were performed on a PSSM-8 (Shimadzu) system with computer-assisted operation on a 20 μmol scale using Fmoc chemistry.

4.2 HAT inhibitor-PIP synthesis

Machine-assisted automatic solid-phase synthesis of hairpin-type PIP was carried out with the use of a continuous-flow peptide synthesizer (PSSM-8, Shimadzu, Kyoto, Japan) at 0.1 mmol scale (100 mg of Fmoc oxime resin, 0.50 meq/g, Peptide Institute, Osaka, Japan) [15]. In a stepwise reaction, Fmoc-Py-COOH, Fmoc-Im-COOH, Fmoc-Py–Im-COOH, Fmoc-β-alanine-COOH, 4-(Fmoc-amino) butyric acid and Fmoc-4,7-dioxanonanoic acid were

coupled sequentially. Automatic solid-phase synthesis was started by washing with dimethylformamide (DMF); coupling with a monomer for 60 min in an environment of 1-[bis(dimethylamino)methylene]- 5-chlorobenzotriazolium 3-oxide hexafluorophosphate (HCTU) and diisopropylethylamine (4 eq. each); removing the Fmoc group using 20% piperidine/DMF. We then isolated PIP after cleavage step (1 ml *N*,*N*-Dimethylpropylamine) for compounds **1-4**.

Through 11-step solid phase synthesis and reverse-phase flash column, four PIPs were successfully synthesized. Then, our target compounds were synthesized and purified in high yield by conjugating commercially available C646 with **1-NH$_2$**, **2-NH$_2$**, **3-NH$_2$,** and **4-NH$_2$** respectively with the help of coupling agent PyBOP. To purify the PIP conjugates, high performance liquid chromatography (HPLC) was performed with use of a PU-980 HPLC pump, UV-975 HPLC UV/VIS detector (Jasco, Easton, MD), and Chemcobound 5-ODS-H column (Chemco Scientific, Osaka, Japan). ESI-MS data are listed in Supplementary Data **S7-S11**.

PIP-I was obtained as a white powder. MS (ESI-TOF): *m*/*z* calcd for $C_{57}H_{71}N_{21}O_{10}^{2+}$ $[M+2H]^{2+}$: 604.7841; found: 604.7302; HPLC: t_R=16.09 min (0.1 % TFA/MeCN, linear gradient 0–100 %, 0–40 min).

1-NH$_2$ was obtained as a white powder. MS (ESI-TOF): *m*/*z* calcd for $C_{61}H_{77}N_{23}O_{11}^{2+}$ $[M+2H]^{2+}$: 654.8159; found: 654.6877; HPLC: t_R=10.06 min (0.1 % TFA/MeCN, linear gradient 0–100 %, 0–20 min).

2-NH$_2$ was obtained as a white powder. MS (ESI-TOF): *m*/*z* calcd for $C_{64}H_{85}N_{23}O_{13}^{2+}$ $[M+2H]^{2+}$: 691.8343; found: 691.6911; HPLC: t_R=10.11 min (0.1 % TFA/MeCN, linear gradient 0–100 %, 0–20 min).

3-NH$_2$ was obtained as a white powder. MS (ESI-TOF): *m*/*z* calcd for $C_{67}H_{91}N_{23}O_{15}^{2+}$ $[M+2H]^{2+}$: 728.8527; found: 728.7889; HPLC: t_R=10.18 min (0.1 % TFA/MeCN, linear gradient 0–100 %, 0–20 min).

4-NH$_2$ was obtained as a white powder. MS (ESI-TOF): *m*/*z* calcd for $C_{63}H_{84}N_{24}O_{13}^{2+}$ $[M+2H]^{2+}$: 692.3320; found: 692.3352; HPLC: t_R=9.692 min (0.1 % TFA/MeCN, linear gradient 0–100 %, 0–20 min).

1 was obtained as a red powder. MS (ESI-TOF): *m*/*z* calcd for $C_{85}H_{96}N_{26}O_{16}^{2+}$ $[M+2H]^{2+}$: 868.3744; found: 868.2229; HPLC: t_R=14.05 min (0.1 % TFA/MeCN, linear gradient 0–100 %, 0–20 min).

2 was obtained as a red powder. MS (ESI-TOF): *m*/*z* calcd for $C_{88}H_{102}N_{26}O_{18}^{2+}$ $[M+2H]^{2+}$: 905.3927; found: 905.3164; HPLC: t_R=14.10 min (0.1 % TFA/MeCN, linear gradient 0–100 %, 0–20 min).

3 was obtained as a red powder. MS (ESI-TOF): *m*/*z* calcd for $C_{91}H_{108}N_{26}O_{20}^{2+}$ $[M+2H]^{2+}$: 942.4111; found: 942.4408; HPLC: t_R=14.19 min (0.1 % TFA/MeCN, linear gradient 0–100 %, 0–20 min).

4 was obtained as a red powder. MS (ESI-TOF): *m*/*z* calcd for $C_{87}H_{101}N_{27}O_{18}^{2+}$ $[M+2H]^{2+}$: 905.8904; found: 906.0553; HPLC: t_R=13.83 min (0.1 % TFA/MeCN, linear gradient 0–100 %, 0–20 min).

Polyamide concentrations were calculated with a Nanodrop ND-1000 spectrophotometer (Thermo Fisher Scientific Inc.) using an extinction coefficient of 9900 M1 cm^{-1} per one pyrrole or imidazole moiety at λ_{max} near 310 nm [16]. C646-PIP concentrations were

calibrated by comparing UV absorbance at 410 nm to C646 [13].

4.3 Thermal stability assay

Thermal stabilization of polyamide–DNA complex can be analyzed by thermal melting temperature (T_m) analysis, and this method has been used for the measurement of the relative binding affinity and the ability to discriminate mismatch sequences. Melting temperature analyses were performed on a spectrophotometer V-650 (JASCO) equipped with a thermos-controlled PAC-743R cell changer (JASCO), a refrigerated, and heating circulator F25-ED (Julabo). The sequences of dsDNA were ODN1: 5'-ACTTATTCCATATAGA-3', ODN2: 3'-TGAATAAGGTATATCT-5', ODN3: 5'-ACTTATCCACTATAGA-3', and ODN4: 3'-TGAATAGGTGATATCT-5'. The underlined bases were the binding sites of polyamides. The analysis buffer was the aqueous solution of 10 mM NaCl and 10 mM sodium cacodylate at pH 7.0 containing 0.25 % v/v DMF. The concentration of polyamides and dsDNA was 2.5 μM, respectively. Before analyses, samples were annealed from 95 ℃to 20 ℃ at a rate of 1.0 ℃/min. Denaturation profiles were recorded at λ= 260 nm from 20 to 95 ℃ at a rate of 1.0 ℃/min.

4.4 HAT activity assay in vitro

HAT activity assays were determined using a commercial available kit (Biovision Biotechnology) according to the manufacturer's instruction [12]. Biovision's HAT Activity Assay Kit utilizes Acetyl CoA and H3 histone peptide as substrates, and recombinant p300 core domain as the enzyme. In this assay, HAT enzyme catalyzes the transfer of acetyl groups from Acetyl-CoA to the histone peptide, thereby generating two products - acetylated peptide and CoA-SH. The CoA-SH reacts with the developer to generate a product that is detected fluorometrically at Ex/Em = 535/587 nm.

4.5 Cell culture

To make the complete growth medium for A549 cell line: ATCC-formulated DMEM medium, fetal bovine serum (Sigma FBS) to a final concentration of 10% and L-glutamine to a final percentage of 2 mM. To make the complete growth medium for MV4-11 cell line: RPMI 1640 medium, FBS to a final concentration of 10%, L-glutamine to a final percentage of 2 Mm and penicillin/streptomycin to a final concentration of 1%. To make the complete growth medium for SW620 cell line, we added the following components to the base medium: ATCC-formulated DMEM medium, FBS to a final concentration of 10% and penicillin/streptomycin to a final concentration of 1%. To make the complete growth medium for SW620 cell line, we added the following components to the base medium: ATCC-formulated DMEM medium, FBS to a final concentration of 10% and penicillin/streptomycin to a final concentration of 1%. To make the complete growth medium for MDA-MB-231 cell line, we added the following components to the base medium: ATCC-formulated DMEM medium, FBS to a final concentration of 10% and penicillin/streptomycin to a final concentration of 1%.

4.6 Cell proliferation assay

Cancer cell lines were seeded on 96-well microplates (5×10^3 cells/well) in above mentioned

media for 24 h at 37°C in 5% CO_2. Then media was replenished with varying concentrations of conjugates C646-PIP for 96 h. Count Reagent SF (Nacalai Tesque) was added to each well to evaluate the cell proliferation. The absorbance of each well was measured at 450 nm by SpectraMax M2 (Molecular devices) microplate reader.

4.7 Microarray analysis and data processing

A549 cells were plated in 6-well plates at 2×10^5 cells/well and were treated for 48 h with DMSO (0.01% control) and 2 μM concentration of C646-PIP, with technical duplicates in each condition respectively. Total RNA was prepared and the integrity of the RNA was checked using the Agilent 2100 Bioanalyzer (Agilent Technologies). One hundred nanograms of total RNA quantified by Nanodrop ND1000 v. 3.5.2 (Thermo Scientific) was labeled using a GeneChip WT PLUS Reagent kit (Affymetrix) and was hybridized to Human Gene 2.1 ST Array Strip (Affymetrix) for 20 ± 1 h at 48°C. The hybridized arrays were washed, stained, and imaged on a GeneAtlas Personal Microarray System (Affymetrix). The hybridized probe set values were normalized using Affymetrix gene expression console software. Significant differentially expressed genes between the different conditions were analyzed using *t* test statistics ($p<0.05$). Microarray data reported here were deposited in the Gene Expression Omnibus database under the accession number (currently unavailable).

Gene set enrichment analysis (GSEA) was conducted to detect statistically significant **2** targeted genes associated with a gene set p53-regulated genes. Data were further analyzed by IPA (Ingenuity Systems; http://www.ingenuity.com) [26]. The IPA functional analysis was conducted to identify the significant biological functions associated with the microarray data set. Genes from the data sets that were regulated by ≥1.8-fold cutoff at $p<0.05$ were considered for the analysis. The *p* value was calculated using right-tailed Fisher's exact test that defines the degree of association of the data set to the assigned biological function.

4.8 Apoptosis Detection assay

The apoptosis detection assay was performed using an Apoptotic, Necrotic, and Healthy Cells Detection Kit (Promokine) according to manufacturer's instructions [29]. A549 cells were cultured in 8-well chamber slides at a density of 2×10^4 cells/well and treated with 2 μM PIP for 48 hr. Cells were washed with a binding buffer and stained with FITC-Annexin V, Ethidium Homodimer III, and Hoechst 33342; then they were subjected to fluorescence microscopy analysis (SpectraMax M2, Molecular Devices).

4.8 Statistical analysis

Results for continuous variables were presented as the mean ± standard error. Two-group differences in continuous variables were assessed by the unpaired T-test. *P*-values are two-tailed with confidence intervals of 95%. Statistical analysis was performed by comparing treated samples with untreated controls.

Acknowledgments

This work was supported by JSPS KAKENHI Grant NO. JP16H06356, "Basic Science and Platform Technology Program for Innovative Biological Medicine by Japan Agency for Medical Research and Development (AMED)", "the Platform Project for Supporting Drug Discovery and

Life Science Research funded by AMED" and "JSPS-NSF International Collaborations in Chemistry (ICC)" to G.N.P., Grant NO. 16K12896. We also thank China Scholarship Council (CSC) support Z. Y., Japanese Government (MONBUKAGAKUSHO: MEXT) Scholarship support Y. W., and JSPS scholarship support J. T.

Appendix A. Supplementary data

Supplementary data related to this article can be found at http://dx.doi.org/.

References

[1] A.P. Feinberg, M.A. Koldobskiy, A. Gondor, Epigenetic modulators, modifiers and mediators in cancer aetiology and progression, Nat. Rev. Genet. 17 (2016) 284-299.

[2] M. Mottamal, S.L. Zheng, T.L. Huang, G.D. Wang, Histone Deacetylase Inhibitors in Clinical Studies as Templates for New Anticancer Agents, Molecules 20 (2015) 3898-3941.

[3] S. Castellano, C. Milite, A. Feoli, M. Viviano, A. Mai, E. Novellino, A. Tosco, G. Sbardella, Identification of Structural Features of 2-Alkylidene-1,3-Dicarbonyl Derivatives that Induce Inhibition and/or Activation of Histone Acetyltransferases KAT3B/p300 and KAT2B/PCAF, ChemMedChem 10 (2015) 144-157.

[4] K.C. Ravindra, B.R. Selvi, M. Arif, B.A. Reddy, G.R. Thanuja, S. Agrawal, S.K. Pradhan, N. Nagashayana, D. Dasgupta, T.K. Kundu, Inhibition of lysine acetyltransferase KAT3B/p300 activity by a naturally occurring hydroxynaphthoquinone, plumbagin, J. Biol. Chem. 284 (2009) 24453-24464.

[5] E.M. Bowers, G. Yan, C. Mukherjee, A. Orry, L. Wang, M.A. Holbert, N.T. Crump, C.A. Hazzalin, G. Liszczak, H. Yuan, C. Larocca, S.A. Saldanha, R. Abagyan, Y. Sun, D.J. Meyers, R. Marmorstein, L.C. Mahadevan, R.M. Alani, P.A. Cole, Virtual Ligand Screening of the p300/CBP Histone Acetyltransferase: Identification of a Selective Small Molecule Inhibitor, Chem. Biol. 17 (2010) 471-482.

[6] G.N. Pandian, J. Taniguchi, S. Junetha, S. Sato, L. Han, A. Saha, C. AnandhaKumar, T. Bando, H. Nagase, T. Vaijayanthi, R.D. Taylor, H. Sugiyama, Distinct DNA-based epigenetic switches trigger transcriptional activation of silent genes in human dermal fibroblasts, Sci. Rep. 4 (2014) e3843.

[7] L. Han, G.N. Pandian, S. Junetha, S. Sato, C. Anandhakumar, J. Taniguchi, A. Saha, T. Bando, H. Nagase, H. Sugiyama, A synthetic small molecule for targeted transcriptional activation of germ cell genes in a human somatic cell, Angew. Chem. Int. Ed. 52 (2013) 13410-13413.

[8] G.N. Pandian, K. Shinohara, A. Ohtsuki, Y. Nakano, M. Masafumi, T. Bando, H. Nagase, Y. Yamada, A. Watanabe, N. Terada, S. Sato, H. Morinaga, H. Sugiyama, Synthetic small molecules for epigenetic activation of pluripotency genes in mouse embryonic fibroblasts, Chembiochem 12 (2011) 2822-2828.

[9] S. White, J.W. Szewczyk, J.M. Turner, E.E. Baird, P.B. Dervan, Recognition of the four Watson-Crick base pairs in the DNA minor groove by synthetic ligands, Nature 391 (1998) 468-471.

[10] G.N. Pandian, Y. Nakano, S. Sato, H. Morinaga, T. Bando, H. Nagase, H. Sugiyama, A synthetic small molecule for rapid induction of multiple pluripotency genes in mouse embryonic fibroblasts, Sci. Rep. 2 (2012) e544.

[11] G.N. Pandian, S. Sato, C. Anandhakumar, J. Taniguchi, K. Takashima, J. Syed, L. Han, A. Saha, T. Bando, H. Nagase, H. Sugiyama, Identification of a small molecule that turns ON the pluripotency gene circuitry in human fibroblasts, ACS Chem. Biol. 9 (2014) 2729-2736.

[12] L. Han, G.N. Pandian, A. Chandran, S. Sato, J. Taniguchi, G. Kashiwazaki, Y. Sawatani, K.

Hashiya, T. Bando, Y. Xu, X. Qian, H. Sugiyama, A Synthetic DNA-Binding Domain Guides Distinct Chromatin-Modifying Small Molecules to Activate an Identical Gene Network, Angew. Chem. Int. Ed. Engl. 54 (2015) 8700-8703.

[13] J.H. Shrimp, A.W. Sorum, J.M. Garlick, L. Guasch, M.C. Nicklaus, J.L. Meier, Characterizing the Covalent Targets of a Small Molecule Inhibitor of the Lysine Acetyltransferase P300, ACS Med. Chem. Lett. 7 (2016) 151-155.

[14] G.N. Pandian, A. Ohtsuki, T. Bando, S. Sato, K. Hashiya, H. Sugiyama, Development of programmable small DNA-binding molecules with epigenetic activity for induction of core pluripotency genes, Bioorg. Med. Chem. 20 (2012) 2656-2660.

[15] H. Morinaga, T. Bando, T. Takagaki, M. Yamamoto, K. Hashiya, H. Sugiyama, Cysteine cyclic pyrrole-imidazole polyamide for sequence-specific recognition in the DNA minor groove, J. Am. Chem. Soc. 133 (2011) 18924-18930.

[16] C. Guo, Y. Kawamoto, S. Asamitsu, Y. Sawatani, K. Hashiya, T. Bando, H. Sugiyama, Rational design of specific binding hairpin Py-Im polyamides targeting human telomere sequences, Bioorg. Med. Chem. 23 (2015) 855-860.

[17] C. Guo, S. Asamitsu, G. Kashiwazaki, S. Sato, T. Bando, H. Sugiyama, DNA Interstrand Crosslinks by H-pin Polyamide (S)-seco-CBI Conjugates, ChemBioChem 18 (2017) 166-170.

[18] K. Balasubramanyam, V. Swaminathan, A. Ranganathan, T.K. Kundu, Small molecule modulators of histone acetyltransferase p300, J. Biol. Chem. 278 (2003) 19134-19140.

[19] G.-B. Li, L.-Y. Huang, H. Li, S. Ji, L.-L. Li, S.-Y. Yang, Identification of new p300 histone acetyltransferase inhibitors from natural products by a customized virtual screening method, RSC Adv 6 (2016) 61137-61140.

[20] X.-n. Gao, J. Lin, Q.-y. Ning, L. Gao, Y.-s. Yao, J.-h. Zhou, Y.-h. Li, L.-l. Wang, L. Yu, A Histone Acetyltransferase p300 Inhibitor C646 Induces Cell Cycle Arrest and Apoptosis Selectively in AML1-ETO-Positive AML Cells, PLoS ONE 8 (2013) e55481.

[21] T. Oike, M. Komachi, H. Ogiwara, N. Amornwichet, Y. Saitoh, K. Torikai, N. Kubo, T. Nakano, T. Kohno, C646, a selective small molecule inhibitor of histone acetyltransferase p300, radiosensitizes lung cancer cells by enhancing mitotic catastrophe, Radiother. Oncol. 111 (2014) 222-227.

[22] G. Kashiwazaki, T. Bando, T. Yoshidome, S. Masui, T. Takagaki, K. Hashiya, G.N. Pandian, J. Yasuoka, K. Akiyoshi, H. Sugiyama, Synthesis and Biological Properties of Highly Sequence-Specific-AlkylatingN-Methylpyrrole–N-Methylimidazole Polyamide Conjugates, J. Med. Chem. 55 (2012) 2057-2066.

[23] F. Yang, N.G. Nickols, B.C. Li, G.K. Marinov, J.W. Said, P.B. Dervan, Antitumor activity of a pyrrole-imidazole polyamide, Proc. Natl. Acad. Sci. U.S.A. 110 (2013) 1863-1868.

[24] H. Piotrowska-Kempisty, M. Rucinski, S. Borys, M. Kucinska, M. Kaczmarek, P. Zawierucha, M. Wierzchowski, D. Lazewski, M. Murias, J. Jodynis-Liebert, 3 '-hydroxy-3,4,5,4 '-tetramethoxystilbene, the metabolite of resveratrol analogue DMU-212, inhibits ovarian cancer cell growth in vitro and in a mice xenograft model, Sci. Rep. 6 (2016).

[25] A. Krämer, J. Green, J. Pollard, S. Tugendreich, Causal analysis approaches in ingenuity pathway analysis (ipa), Bioinformatics 30 (2013) 523-530.

[26] V.K. Mootha, C.M. Lindgren, K.F. Eriksson, A. Subramanian, S. Sihag, J. Lehar, P. Puigserver, E. Carlsson, M. Ridderstrale, E. Laurila, N. Houstis, M.J. Daly, N. Patterson, J.P. Mesirov, T.R. Golub, P. Tamayo, B. Spiegelman, E.S. Lander, J.N. Hirschhorn, D. Altshuler, L.C. Groop, PGC-1alpha-responsive genes involved in oxidative phosphorylation are coordinately downregulated in

human diabetes, Nat. Genet. 34 (2003) 267-273.

[27] M. Wade, Y.-C. Li, G.M. Wahl, MDM2, MDMX and p53 in oncogenesis and cancer therapy, Nat. Rev. Cancer. 13 (2013) 83-96.

[28] H. Hong, K. Takahashi, T. Ichisaka, T. Aoi, O. Kanagawa, M. Nakagawa, K. Okita, S. Yamanaka, Suppression of Indued Pluripotent Stem Cell Generation by the p53-p21 Pathway, Nature 460 (2009) 1132-1135.

[29] J. Syed, A. Chandran, G.N. Pandian, J. Taniguchi, S. Sato, K. Hashiya, G. Kashiwazaki, T. Bando, H. Sugiyama, A Synthetic Transcriptional Activator of Genes Associated with the Retina in Human Dermal Fibroblasts, Chembiochem 16 (2015) 1497-1501.

[30] D. Hanahan, R.A. Weinberg, Hallmarks of cancer: the next generation, Cell 144 (2011) 646-674.

[31] K.T. Bieging, S.S. Mello, L.D. Attardi, Unravelling mechanisms of p53-mediated tumour suppression, Nat. Rev. Cancer. 14 (2014) 359-370.

[32] R. Aloni-Grinstein, Y. Shetzer, T. Kaufman, V. Rotter, p53: The barrier to cancer stem cell formation, FEBS Lett. 588 (2014) 2580-2589.

[33] F.T. Merkle, S. Ghosh, N. Kamitaki, J. Mitchell, Y. Avior, C. Mello, S. Kashin, S. Mekhoubad, D. Ilic, M. Charlton, G. Saphier, R.E. Handsaker, G. Genovese, S. Bar, N. Benvenisty, S.A. McCarroll, K. Eggan, Human pluripotent stem cells recurrently acquire and expand dominant negative P53 mutations, Nature 545 (2017) 229-233.

Graphical abstract

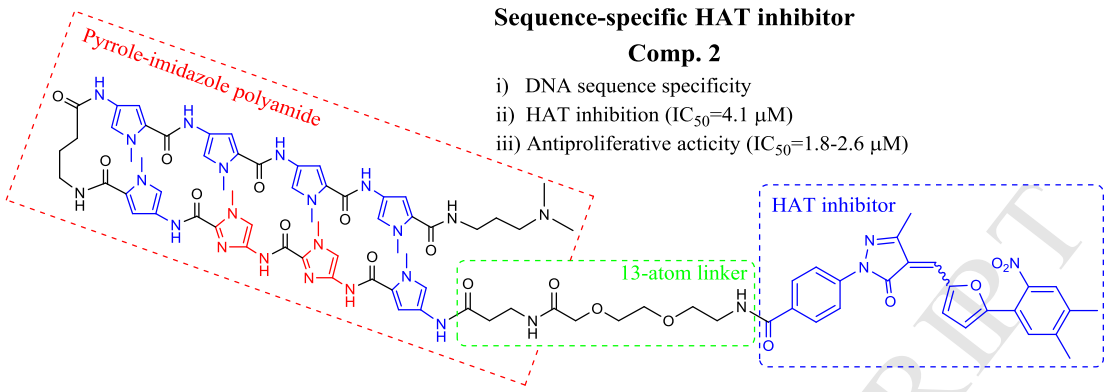

Highlights

- Sequence-specific HAT inhibitors C646-PIP were reported here for the first time and predicted working assay, including thermal stability assay and in vitro HAT activity assay, showed these conjugates retained dual-targeting activities;
- In p53 wild-type cancer cell lines, **2** which contains medium linker length of 13-atom and **PIP-I** sequence was identified with highest antiproliferative activity with an IC_{50} of 1.8-2.6 μM in A549 and MV4-11 cells;
- Highly regulated p53 downstream targets and cancer cell apoptosis contribute to antiproliferative activity of **2**.